An independent component analysis based filter design for defect detection in low-contrast surface images

by

Du-Ming Tsai, Ping-Chieh Lin and Chi-Jie Lu
Department of Industrial Engineering and Management
Yuan-Ze University, Taiwan, R.O.C.

Correspondence:

Du-Ming Tsai
Department of Industrial Engineering & Management
Yuan-Ze University
135 Yuan-Tung Road
Nei-Li, Tao-Yuan
Taiwan, R.O.C.

Fax: (03) 463-8907
E-mail: iedmtsai@saturn.yzu.edu.tw

An independent component analysis based filter design for defect detection in low-contrast surface images

Abstract

In this paper, we propose a convolution filtering scheme for detecting small defects in low-contrast uniform surface images and, especially, focus on the applications for backlight panels and glass substrates found in Liquid Crystal Display (LCD) manufacturing. A defect embedded in a low-contrast surface image shows no distinct intensity from its surrounding region, and even worse, the sensed image may present uneven brightness on the surface. All these make the defect detection in low-contrast surface images extremely difficult.

In this study, a constrained ICA (independent component analysis) model is proposed to design an optimal filter with the objective that the convolution filter will generate the most representative source intensity of the background surface without noise. The prior constraint incorporated in the ICA model confines the source values of all training image patches of a defect-free image within a small interval of control limits. In the inspection process, the same control parameter used in the constraint is also applied to set up the thresholds that make impulse responses of all pixels in faultless regions within the control limits, and those in defective regions outside the control limits. A stochastic evolutionary computation algorithm, particle swarm optimization (PSO), is applied to solve for the constrained ICA model. Experimental results have shown that the proposed method can effectively detect small defects in low-contrast backlight panels and LCD glass substrate images.

Keyword: Defect detection, Surface inspection, Independent component analysis, Convolution filter; Particle swarm optimization

1. Introduction

Image analysis techniques are being increasingly used to automate industrial inspection. The manual activity of inspection could be subjective and highly dependent on the experience of human personnel. Subtle defects appearing in a low-contrast surface cannot be visibly identified even with a well-trained inspector. In automatic surface inspection, small defects which appear as local anomalies embedded in a homogeneous surface must be reliably detected. This paper considers the issue of designing a convolution filter for defect detection in low-contrast surface images using Independent Component Analysis (ICA).

Defect detection in uniform surface images arises in glass plate [1], sheet steel [2], aluminum strips [3] and web materials [4]. Most of the existing defect detection methods for uniform surfaces use simple thresholding or edge detection techniques. Defects in these images can be easily detected because they commonly have distinctly measured values with respect to those of the uniform background. The inspection task in the present paper is the detection of subtle defects in uniform surfaces that involve low-contrast intensities in images. This type of surfaces arises in many industrial materials. In this paper, we especially aim at backlight panels and glass substrates in Thin Film Transistor-Liquid Crystal Display (TFT-LCD) manufacturing.

In recent years, there is a great demand for flat-panel displays used as monitors for notebook and personal computers, and as viewfinders for handheld devices such as cellular phones and PDAs. TFT-LCDs have become increasingly important as one of flat panel display devices due to their full-color display capabilities, low power consumption and light weight. The backlight unit and LCD glass substrate are two

important components composing a TFT-LCD module. The inspection of defects in such panel surfaces ensures the display quality and improves the yield in LCD manufacturing. Most of the existing machine vision algorithms for defect inspection in LCD panel surfaces are still mainly based on thresholding, edge detection and first-order statistics [5] such as mean and variance from the gray-level histogram of an image. Kim *et al.* [6] presented an automated inspection algorithm for detecting spot-type defects in TFT-LCD panels. An adaptive multi-level thresholding method that uses the statistical characteristics of the local area is applied for adaptive segmentation of spot-type defects. Saitoh [7] proposed a machine vision system for the inspection of LCD brightness unevenness. An edge detection algorithm was first used to detect discontinuous points. A genetic algorithm was then applied to extract the visual continuous boundary of a non-uniform brightness region for distinguishing true defects from noise. Jiang *et al.* [8] used a luminance meter, instead of a CCD camera, as the sensing device for detecting brightness unevenness in LCD panels. Analysis of variance (ANOVA) and exponentially weighted moving average techniques were applied to determine the presence of region-type defects. Sokolov and Treskunov [9] developed an automatic vision system for final output checks of LCDs. Their method was mainly based on the brightness distribution of an LCD image. It compares the average brightness of background between a reference LCD image and an inspection image to detect the appearance of defects.

In low-contrast surfaces, a local anomaly has smooth change of brightness from its surrounding region and, therefore, has no clear edges to apply the gradient-based methods for defect detection. The non-uniform intensity of a faultless region and the low-contrast intensity of a defective region also deter the use of simple thresholding methods. It is extremely difficult to reliably identify real defects in low-contrast

surface images without false detection of noise. Lee and Yoo [10] proposed a complicated data fitting approach for detecting regional defects of brightness unevenness. They first estimated the background surface of an inspection image using a low-order polynomial data fitting. Subtraction of the estimated background surface from the original image is then applied to find the threshold for binary segmentation. The resulting image is then post-processed by median filtering, morphological closing and opening to remove noise and refine the segmentation. The proposed method worked successfully to detect regional defects in low-contrast TFT-LCD surface images. However, it is very computationally intensive because the background surface must be estimated recursively by eliminating one pixel at a time throughout the entire inspection image.

In this paper, we propose a convolution filtering scheme for defect detection in low-contrast uniform surface images. The design of the convolution filter is based on independent component analysis with the goal that the resulting impulse responses are consistently the same for pixels in faultless regions and distinctly different for pixels in defective regions. ICA is a novel statistical signal process technique to extract independent sources given only observed data that are mixtures of the unknown sources, without any prior knowledge of the mixing mechanisms [11, 12]. The observed signals are generally assumed to be a linear mixture of the unknown sources from a mixing matrix which is solved by maximizing the independency of the estimated source signals. The estimated source signals are termed independent components (ICs), and the inverse of the mixing matrix is called de-mixing matrix.

ICA has been widely applied in medical signal processing such as EEG, fMRI and MEG data [13-17], and audio signal processing [18, 19] for the purpose of signal

de-noising and extraction of meaningful sources for interpretation. It also has been applied in face recognition [20-23] and texture analysis [24-26] that used either the estimated independent components or the corresponding column vectors of the mixing matrix (or row vectors of the de-mixing matrix) as features for classification. Hyvarinen *et al*. [27, 28], Hyvarinen [29] and Hung and Luo [30] used ICA for image denoising. They applied the ICA algorithm and maximum a posteriori (MAP) estimator in a noise-free training image to find the mixing matrix. The mixing matrix is then used in a sensed image to obtain the noisy ICs. The shrinkage nonlinearity function is applied to remove noise in the noisy ICs. The filtered ICs were finally multiplied with the mixing matrix to restore the image.

In this study, ICA is used to design an optimal filter in the sense that the filter will generate the most representative source intensity of the background surface without noise so that all pixels in faultless regions have approximately the same impulse responses, while the pixels in defective regions have distinct responses in the filtered image. In an ICA model, independent components and the mixing matrix that constructs the observed signals can be estimated from the training samples by maximizing the independency of the estimated sources. Since any training image patches of the same size as the filter in a faultless surface image can be treated as translated versions of the same pattern, only one source is needed to be estimated in this study. The corresponding row vector of the estimated source in the de-mixing matrix is used as the convolution filter for defect detection in low-contrast uniform surface images.

An ICA model with a prior constraint is applied to determine the filter so that the impulse responses of all training image patches are as consistent as possible. The

constraint incorporated in the ICA model is given by the upper and lower control limits defined by the mean and standard deviation of the resulting impulse responses of all image patches used in training. In this study, we propose a stochastic optimization procedure based on the Particle Swarm Optimization (PSO) algorithm to effectively determine the de-mixing row vector, i.e. the convolution filter, of the constrained ICA model. In the inspection process, the same parameter value of the control limits used as the constraint in the training process is conveniently adopted to set up the thresholds for segmenting defects from the background surface. The convolution filter will give an impulse response within the control limits when the sliding window of the filter spans a regular region in the inspection image, and will generate a distinct impulse response outside the control limits for a defective region. This transforms the low image difference into a detectable filter output.

Two types of low-contrast surfaces, backlight panels and glass substrates found in LCD manufacturing, are the main application targets of the proposed method. Figures 1(a1) and (b1) show, respectively, a faultless backlight panel image and a defective one. The subtle defect is nearly invisible in the low-contrast image. Figures 1(a2) and (b2) illustrate the respective enhanced images by linearly stretching the original gray levels in Figures 1(a1) and (b1) between 0 and 255 for an 8-bit display. The subtle defect is now much better visible in the enhanced image of Figure 1(b2). Owing to the inherent structural pattern on the backlight panel surface, the enhanced images turn into structurally textured images with uneven illumination. The task of defect detection in such an enhanced image becomes difficult because it is hard to distinguish defects from noise in a textured image with non-uniform illumination. Figures 1(a3) and (b3) present the gradient images of Figures 1(a1) and (b1), respectively. The resulting images reveal that the characteristic of a low-contrast

surface image invalidates the use of gradient magnitude to identify a defect without false alarms of noise.

This paper is organized as follows: Section 2 first discusses the convolution filtering approach for defect detection in uniform surface images. The basic ICA model is then overviewed. The constrained ICA model used for the design of the convolution filter is next introduced. The PSO search algorithm that determines the best filter coefficients from the constrained ICA model is finally presented. Section 3 demonstrates the experimental results from a number of backlight panels and LCD glass substrates containing various local defects. The impact of the constraint setup in the ICA model, and the effect of changes in filter size are also evaluated in this section. The paper is concluded in Section 4.

2. The proposed ICA filtering scheme

2.1 Convolution filtering

In this study, we propose a filtering approach for defect detection in low-contrast surface images. The advantages of the filtering method for defect inspection are threefold: 1) its implementation is simple and straightforward in the inspection process since it involves only simple convolution operations; 2) it takes only one filter to detect various unanticipated defects in a uniform surface image; 3) it converts the difficult qualitative measures of ill-defined defects into a simple detectable impulse response. To fulfill all the benefits of the filtering method in the inspection process, it relies on the design of an optimal filter with the objective that the impulse responses of all pixels in defective regions are highly distinct from those in faultless regions in an image.

Let $f(x, y)$ be the gray level at pixel coordinates (x, y) in an inspection image of size $M \times N$, and $h(i, j)$ the filter of size $m \times n$. The impulse response $r(x, y)$ at point (x, y) is given by convolving an image patch of size $m \times n$ with the filter, i.e.

$$r(x, y) = \sum_{i=0}^{m-1} \sum_{j=0}^{n-1} f(x + i, y + j) \cdot h(i, j) \tag{1}$$

The convolution filter slides over the entire inspection image pixel by pixel so that the impulse response of every pixel in the image can be evaluated. If the resulting impulse responses of defective pixels are distinctly different from those of faultless pixels, the statistical process control principle can be simply used to set up the control limits (i.e. the thresholds) for distinguishing local anomalies from the uniform background in the filtered image. The upper and lower control limits for response magnitude variation in the filtered image are given by

$$\mu_r \pm K\sigma_r \tag{2}$$

where μ_r and σ_r are the mean and standard deviation of impulse responses in the filtered image of size $M \times N$, i.e.

$$\mu_r = \frac{1}{M \cdot N} \sum_x \sum_y r(x, y)$$

$$\sigma_r = \left\{ \frac{1}{M \cdot N - 1} \sum_x \sum_y [r(x, y) - \mu_r]^2 \right\}^{1/2}$$

K is a control constant, and is generally given by 3 to follow the statistical 3-sigma standard.

In this study, a constrained version of ICA model is used to determine the best convolution filter for defect detection in low-contrast surface images. The basic ICA model is initially overviewed in the following subsection.

2.2 The basic ICA model

In the basic ICA model [12, 31], the observed mixture signals $\boldsymbol{X}$ can be expressed as

$$\boldsymbol{X} = \boldsymbol{AS} \tag{3}$$

where $\boldsymbol{A}$ is an unknown mixing matrix; $\boldsymbol{S}$ represents the latent source signals, meaning that they cannot be directly observed from the mixture signals $\boldsymbol{X}$. The ICA model describes how the observed mixture signals $\boldsymbol{X}$ are generated by a process that uses the mixing matrix $\boldsymbol{A}$ to mix the latent source signals $\boldsymbol{S}$. The source signals are assumed to be mutually statistically independent. Based on the assumption, the ICA solution is obtained in an unsupervised learning process that finds a de-mixing matrix $\boldsymbol{W}$. The matrix $\boldsymbol{W}$ is used to transform the observed mixture signals $\boldsymbol{X}$ to yield the independent signals, i.e. $\boldsymbol{WX} = \boldsymbol{Y}$. The independent signals $\boldsymbol{Y}$ are used as the estimates of the latent source signals $\boldsymbol{S}$. The components of $\boldsymbol{Y}$, called independent components, are required to be as mutually independent as possible.

Two preprocessing steps are common in ICA, centering and whitening [12, 20]. First, the input matrix $\boldsymbol{X}$ is centered by subtracting the mean of each columns of $\boldsymbol{X}$. The matrix $\boldsymbol{X}$ with zero mean is then passed through the whitening matrix $\boldsymbol{V}$ to remove the second order dependency. The whitening matrix $\boldsymbol{V}$ is twice the inverse square root of the covariance matrix of the input matrix, i.e. $\boldsymbol{V} = 2 \cdot [Cov(\boldsymbol{X})]^{-1/2}$.The rows of the whitened input matrix are uncorrelated and have unit variance. This

means that the variances of the independent components are equalized and have unit variance. In this study, it is assumed that the input matrix $\boldsymbol{X}$ is centered and whitened.

There exist several algorithms performing ICA [32-35]. The objective of the algorithm is to maximize the statistical independency (non-Gaussianity) of the ICs. The non-Gaussianity of the ICs can be measured by the negentropy [12, 31] given by

$$J(\boldsymbol{y}) = H(\boldsymbol{y}_{gauss}) - H(\boldsymbol{y}) \tag{4}$$

where $\boldsymbol{y}_{gauss}$ is a Gaussian random vector of the same covariance matrix as $\boldsymbol{y}$. H is the entropy of a random vector $\boldsymbol{y}$ with density $p_y(\eta)$ defined as

$$H(\boldsymbol{y}) = -\int p_y(\eta)\ log\ p_y(\eta)\, d\eta$$

The negentropy is always non-negative and is zero if and only if $\boldsymbol{y}$ has a Gaussian distribution. It is well justified as an estimator of the non-Gaussianity of the ICs. Since the problem in using negentropy is computationally very difficult, an approximation of negentropy is proposed as follows [12]:

$$J(y) \approx \{E[G(y)] - E[G(v)]\}^2 \tag{5}$$

where v is a Gaussian variable of zero mean and unit variance. G is a non-quadratic function, which is given by $G(y) = -exp(-y^2/2)$ in this study for defect detection applications.

2.3 The constrained ICA model

In order to make the convolution operation of the resulting filter from the ICA model consistent with the linear filtering in eq. (1), each training image patch must be organized as a column vector in the data matrix $\boldsymbol{X}$. Let the convolution filter be of size $m \times n$. We select randomly a training image patch of the same size as the filter from a defect-free surface image, and organize it as a column vector. Let $\boldsymbol{x}_i = [x_{i1}, x_{i2}, \cdots, x_{iR}]^T$ represent the i-th training column vector of the data matrix $\boldsymbol{X}$ = $[\boldsymbol{x}_1, \boldsymbol{x}_2, \cdots, \boldsymbol{x}_C]$, where $R = m \cdot n$ is the total number of pixels in an image patch, and C is the total number of training image patches. $\boldsymbol{x}_i$ is the re-shaped column vector from the i-th training image patch, $i = 1, 2, \cdots, C$. Following the basic ICA model in eq. (3), a column vector $\boldsymbol{x}$ can be expressed as

$$\boldsymbol{x} = \sum_{i=1}^{C} s_i \boldsymbol{a}_i = \boldsymbol{A}\boldsymbol{s} \tag{6}$$

where $\boldsymbol{a}_i, i = 1, 2, \cdots, C$, is the i-th column of the $R \times C$ mixing matrix $\boldsymbol{A}$, and $\boldsymbol{s}$ = $[s_1, s_2, \cdots, s_C]^T$.

ICA aims to find a $C \times R$ de-mixing matrix $\boldsymbol{W}$ of the data $\boldsymbol{x}$ such that

$$\boldsymbol{y} = \boldsymbol{W}\boldsymbol{x} \tag{7}$$

The vector $\boldsymbol{y}$ is an estimate of the source $\boldsymbol{s}$, and its components are as statistically independent as possible.

In this study, the target surfaces to be inspected fall in the class of uniform

images. Any arbitrarily selected training image patches in a faultless surface image are considered to be approximately identical, regardless of their positions in the image. The column images in the data matrix $\boldsymbol{X}$ can thus be treated as the mixture signals from the same single source. If several independent components are estimated from the ICA model, they simply correspond to translated versions of the original source signal. Therefore, it is sufficient to estimate just one component and a single row vector in the de-mixing matrix $\boldsymbol{W}$ for defect detection in uniform surface images. Since we only need to estimate a single source, the $C \times R$ de-mixing matrix $\boldsymbol{W}$ in eq. (7) is now reduced to a $1 \times R$ row vector $\boldsymbol{w}$, and the resulting component vector $\boldsymbol{y}$ becomes a scalar y, i.e.

$$y = \boldsymbol{w}\boldsymbol{x} \tag{8}$$

In the ICA model of eq. (8), source value y can be interpreted as the most representative intensity of a faultless surface used in training. The resulting source image patch can be treated as a constant-intensity image.

Note that the operation in eq. (8) is exactly the same form as the convolution filtering in eq. (1). Thus, the estimated de-mixing vector $\boldsymbol{w}$ is taken as the convolution filter, and the resulting source value y is the impulse response of an image patch $\boldsymbol{x}$ under inspection. Given the data matrix $\boldsymbol{X} = [\boldsymbol{x}_1, \boldsymbol{x}_2, \cdots, \boldsymbol{x}_C]$ that contains C training image patches from a faultless surface image, the resulting source y_i for each training image patch $\boldsymbol{x}_i$, i.e.

$$y_i = \boldsymbol{w}\boldsymbol{x}_i, i = 1, 2, \cdots, C \tag{9}$$

should have the same value since every training image patch is extracted from the same source surface. As mentioned previously in section 2.1, statistical control limits are used as the dual thresholds of impulse response to segment local anomalies from the uniform background. In the search of the best vector $\boldsymbol{w}$ in the training process, we include a constraint in the ICA model so that the resulting de-mixing row vector, i.e. the convolution filter, will generate the least variation of source values y_i. The constraint is also constructed in the same way as the statistical control limits formulated in eq. (2). That is,

$$\max_j\{y_j\} < \mu_y + K\sigma_y$$

and (10)

$$\min_j\{y_j\} > \mu_y - K\sigma_y$$

where y_j is the resulting source value from eq. (9), $j = 1, 2, \cdots, C$;

$\mu_y =$ the mean of $y = \dfrac{1}{C}\sum_{j=1}^{C} y_j$;

$\sigma_y =$ the standard deviation of $y = \left\{\dfrac{1}{C-1}\sum_{j=1}^{C}(y_j - \mu_y)^2\right\}^{1/2}$

$K =$ the control constant, which is user specified. It takes the same value as that of eq. (2) used in the inspection process.

The constraint in eq. (10) restricts the maximum and minimum source values y_i within the upper and lower control limits, respectively. A small control constant value *K* will result in a small deviation of *y* in the training process. The same control constant *K* determined in the training process is conveniently used to set up the dual thresholds in the inspection process. With a tight constraint in the training

process, it is expected that defective image patches will result in highly distinct impulse responses outside the control limits in the inspection process.

In this study, the approximation of negentropy with $G(y) = -exp(-y^2/2)$ is used as the measure of independency. The proposed constrained ICA model for defect detection in uniform surface images are therefore formulated as

$$\text{Maximize } Fitness(\boldsymbol{y}) = \left\{ \frac{1}{C} \sum_{j=1}^{C} [-exp(-y_j^2/2)] \right\}^2 \tag{11}$$

subject to

$$\max_j \{y_j\} < \mu_y + K\sigma_y$$

and

$$\min_j \{y_j\} > \mu_y - K\sigma_y$$

where $\boldsymbol{y} = \boldsymbol{wX} = [y_1, y_2, \cdots y_C]$;

$\boldsymbol{w} = [w_1, w_2, \cdots, w_R]$ is the de-mixing row vector; w_i are the decision variables, i.e. the filter coefficients, yet to be determined.

The model formulated above is a nonlinear, constrained programming problem with multiple continuous variables. The *FastICA* algorithm proposed by Hyvarinen *et al.* [12] has been one of the most popular optimization methods in ICA. *FastICA* is based on a fixed-point iteration scheme for finding a maximum of the negentropy. It cannot be directly extended to solve for the de-mixing matrix in the proposed constrained ICA model. This is because the two constraints in eq. (10) are not differentiable, which make the gradient descent method not workable. The particle

swarm optimization algorithm, which is a recently developed high-performance optimizer, is used in this study to search for the best de-mixing row vector $\boldsymbol{w}$ in the constrained ICA model.

2.4 The PSO procedure

Particle swarm optimization is an evolutionary computation technique originally developed by Kennedy and Eberhart [36]. It has been found to be robust and easily implemented in solving nonlinear optimization problems [37-40]. PSO resembles the social interaction from a school of flying birds. Individuals in a group of flying birds are evolved by cooperation and competition among the individuals themselves through generations [41]. Each individual, named as a "particle", adjusts its flying according to its own flying experience and its companions' flying experience. Each particle with its current position represents a potential solution to the problem in hand. In this study, each particle is treated as a point in an *R*-dimensional space since the de-mixing row vector $\boldsymbol{w}$ is of *R* dimensions.

In PSO, a number of particles, which simulate a group of flying birds, are simultaneously used to find the best fitness in the search space. At each iteration, every particle keeps track of its personal best position by dynamically adjusting its flying velocity. The new velocity is evaluated by its current velocity and the distances of its current position with respect to its previous best local position and the global best position. After a sufficient number of iterations, the particles will eventually cluster around the neighborhood of the fittest solution.

Let the *i*-th particle be represented as $\boldsymbol{w}_i = [w_{i1}, w_{i2}, \cdots, w_{iR}]$. The best previous position, i.e. the position giving the best fitness value, of particle *i* is recorded and

represented as $\boldsymbol{p_i} = [p_{i1}, p_{i2}, \cdots, p_{iR}]$. Assume there are a total of t particles in the PSO. Let $\boldsymbol{p^g} = [p_1^g, p_2^g, \cdots, p_R^g]$ denote by the best particle that gives the current optimal fitness value among all the particles in the population. The rate of the position change, i.e. the velocity, for particle i is represented by $\boldsymbol{v_i} = [v_{i1}, v_{i2}, \cdots, v_{iR}]$. Each particle moves over the search space with a velocity dynamically adjusted according to its historical behavior and its companions. The velocity and position of a particle are updated according to the following equations [36, 42]:

$$v_{ij}^{new} = v_{ij} + c_1 \cdot RND_1 \cdot (p_{ij} - w_{ij}) + c_2 \cdot RND_2 \cdot (p_j^g - w_{ij}) \tag{12a}$$

$$w_{ij}^{new} = w_{ij} + v_{ij}^{new}, \text{ for } i = 1,2,\cdots,t \text{ and } j = 1,2,\cdots,R \tag{12b}$$

where RND_1 and RND_2 are two random numbers in the range between 0 and 1; c_1 and c_2 are two positive constants.

The second term in the right-hand side of the velocity equation in eq. (12a) is interpreted as the "cognition" part, which represents the private thinking of the particle itself. The third term in eq. (12a) is the "social" part, which represents the collaboration among the particles [41, 42]. The two positive constants c_1 and c_2 are the weights used to regulate the acceleration of self-cognition (a local best) and social interaction (a global best). Kennedy and Eberhart [36], and Shi and Eberhart [41] suggested $c_1 = c_2 = 2$ since they are on average make the weights for "cognition" and "social" parts to be 1. They are also the values adopted in this study. The velocity equation in eq. (12a) calculates the particle's new velocity in each dimension according to its previous velocity and the distances of its current position from its own

best experience (i.e. position) and the group's best experience. Then the particle moves toward a new position according to the position update equation in eq. (12b). The performance of each particle is measured by the fitness value, i.e. the objective function value. Since the proposed ICA model involves a constraint, only the positions in the feasible space are recorded when calculating the local best $\boldsymbol{p}_i$ and the global best $\boldsymbol{p}^g$ in the PSO search procedure.

We can now formally present the PSO search procedure for the constrained ICA model. The following symbols are the notation used in the algorithm.

Notation:

$t =$ the number of particles in the swarm

$\boldsymbol{X} =$ the training data matrix

$= [\boldsymbol{x}_1, \boldsymbol{x}_2, \cdots, \boldsymbol{x}_C]$, where C is the number of training image patches

$\boldsymbol{x}_i = [x_{i1}, x_{i2}, \cdots, x_{iR}]^T$

$=$ the i-th column vector of $\boldsymbol{X}$, which is re-shaped from an image patch of size $m \times n$, and therefore $R = m \cdot n$, for $i = 1,2,\cdots,C$

$\boldsymbol{w}_i = [w_{i1}, w_{i2}, \cdots, w_{iR}]$

$=$ the position of particle i, for $i = 1,2,\cdots,t$,

which is the de-mixing row vector, i.e. the decision vector to be estimated.

Note that we only need one source component in this study and, therefore, we need to estimate only one de-mixing row vector for each particle.

Fitness($\boldsymbol{y}$) = the fitness value of $\boldsymbol{y}$

The procedure:

Step 1. Center and whiten the data matrix $\boldsymbol{X}$.

Step 2. Initialize:

Randomly generate the initial position and velocity of each particle *i*

$$\boldsymbol{w}_i = [w_{i1}, w_{i2}, \cdots, w_{iR}]$$

and

$$\boldsymbol{v}_i = [v_{i1}, v_{i2}, \cdots, v_{iR}], \quad \text{for } i = 1,2,\cdots,t.$$

In order to prevent overshoot of the target position, small initial values of w_{ij} and v_{ij} are selected in the ranges of $-0.5 < w_{ij} < 0.5$ and $0 < v_{ij} < 0.1$.

Compute the fitness value of each particle:

$$Fitness(\boldsymbol{y}_i) = \left\{ \frac{1}{C} \sum_{j=1}^{C} [-exp(-y_{ij}^2 / 2)] \right\}^2$$

where $\boldsymbol{y}_i = \boldsymbol{w}_i \boldsymbol{X} = [y_{i1}, y_{i2}, \cdots y_{iC}]$, for $i = 1,2,\cdots,t$.

Determine the local best position of particle *i* and the global best position:

$$\boldsymbol{p}_i = [p_{i1}, p_{i2}, \cdots, p_{iR}] = \boldsymbol{w}_i, \text{ for } i = 1,2,\cdots,t$$

$$\boldsymbol{p}^g = [p_1^g, p_2^g, \cdots, p_R^g] = arg\ \max_i \{Fitness(\boldsymbol{p}_i \cdot \boldsymbol{X})\}$$

Step 3. Update the velocity and position of each particle *i*, for $i = 1,2,\cdots,t$:

$$v_{ij}^{new} = v_{ij} + c_1 \cdot RND_1 \cdot (p_{ij} - w_{ij}) + c_2 \cdot RND_2 \cdot (p_j^g - w_{ij})$$

$$w_{ij}^{new} = w_{ij} + v_{ij}^{new}, \quad \text{for } j = 1,2,\cdots,R$$

Let $\boldsymbol{w}_i^{new} = [w_{i1}^{new}, w_{i2}^{new}, \cdots, w_{iR}^{new}]$.

Swap the new and old velocities and positions by setting

$$v_{ij} = v_{ij}^{new} \text{ and } w_{ij} = w_{ij}^{new}$$

Step 4. Normalize $\boldsymbol{w}_i^{new}$:

$$\boldsymbol{w}_i^{new} \leftarrow \boldsymbol{w}_i^{new} \big/ \| \boldsymbol{w}_i^{new} \|, \quad \text{for } i = 1,2,\cdots,t.$$

Step 5. Evaluate the new fitness values, and update local best positions $\boldsymbol{p}_i$ and the global best position $\boldsymbol{p}^g$:

If $Fitness(\boldsymbol{w}_i^{new} \cdot \boldsymbol{X}) > Fitness(\boldsymbol{p}_i \cdot \boldsymbol{X})$, then let $\boldsymbol{p}_i = \boldsymbol{w}_i^{new}$,

else retain the current value of $\boldsymbol{p}_i$, for $i = 1,2,\cdots,t$.

Let $\boldsymbol{p}^g = arg \max_i \{Fitness(\boldsymbol{p}_i \cdot \boldsymbol{X})\}$.

Step 6. Compute the estimated source $\boldsymbol{y}$ based on the global best position $\boldsymbol{p}^g$:

$$\boldsymbol{y} = \boldsymbol{p}^g \cdot \boldsymbol{X} = [y_1, y_2, \cdots, y_C]$$

Step 7. Evaluate the feasibility of $\boldsymbol{y}$:

If $\max_j \{y_j\} < \mu_y + K\sigma_y$ and $\min_j \{y_j\} > \mu_y - K\sigma_y$,

then store the current best feasible solution with $\boldsymbol{w}^* \leftarrow \boldsymbol{p}^g$.

Otherwise, skip to Step 8.

μ_y and σ_y are the mean and standard deviation of y_i in $\boldsymbol{y}$, and K is a predetermined control constant.

Step. 8. Check for the stopping criterion:

If the maximum number of search iterations is reached, then go to Step 9.

Otherwise, repeat Steps 3 through 8 until the stopping criterion is met.

Step 9. Deliver the solution:

$\boldsymbol{w}^* = [w_1^*, w_2^*, \cdots, w_R^*]$ is the best solution obtained, and is used as the convolution filter for defect detection in this study. If $\boldsymbol{w}^*$ is null, no feasible

solution can be delivered in the PSO search process. The number of search iterations, and/or control constant K may have to increase to find a feasible solution of the constrained ICA model.

PSO is an extremely simple and easily implemented algorithm that can dynamically adjust the current local and global positions with a large number of particles in the swarm to simultaneously find the solution from different positions in the search space. It is well suited for the constrained ICA model that involves typically hundreds of decision variables, even with a small image patch of size 20×20.

The resulting de-mixing row vector $\boldsymbol{w}^* = [w_1^*, w_2^*, \cdots, w_R^*]$ must be converted back to a 2D filter $h(i, j)$ so that the 2D convolution operation of eq. (1) can be followed in the inspection process for a 2D inspection image. For a convolution filter of size $m \times n$, the conversion is given by

$$h(i-1, j-1) = w^*_{(i-1)n+j}$$

for $i = 1,2,\cdots,m$ and $j = 1,2,\cdots,n$.

3. Experimental results

This section presents the experimental results from a number of low-contrast surface images found in backlight panels and LCD glass substrates to evaluate the performance of the proposed ICA-based filter design scheme. The test images in the experiments are 200×200 pixels wide with 8-bit gray levels. In the PSO search

algorithm, the required parameters are set up as follows: the population size (the number of particles) t = 10, the weights $c_1 = c_2 = 2$, and the maximum number of iterations (stopping criterion) is 200. Image patches used in training are of size 20×20, and the total number of image patches to form a data matrix is 100, unless otherwise specified. The training image patches were randomly selected from a faultless surface image. In the inspection process, pixels with impulse responses falling within and outside the control limits are respectively represented by white and black intensities so that the detected defects can be visibly observed and verified in the binarized image.

Figure 2(a) shows a defective backlight panel image, and Figure 2(b) is the enhanced version of the image. It is used to demonstrate the effect of varying values of control constant *K* on detection results. The faultless backlight panel image shown in Figure 1(a) was used as the training image, from which the training image patches were extracted. Figure 3 depicts the plot of the fitness value as a function of iteration number. It can be observed from the figure that the PSO search process converges fast after 150 iterations, and it is the case for all test samples evaluated in this study. Therefore, 200 iterations are considered to be sufficient for our problem.

Table 1 summarizes the resulting standard deviation σ_y of the 100 training image patches extracted from Figure 1(a1) and the corresponding maximum fitness value for each individual control constant value of *K*. As expected, the standard deviation σ_y decreases when the value of the control constant *K* used to set up the constraint in training is decreased. The uncontrained ICA model (i.e. $K = \infty$) generates the largest variation of source values *y*, and the largest fitness value. Figures 2(c)-(f) illustrate the detection results of the defective surface image in Figure 2(a)

from control constant K = 2.5, 3.0, 3.5 and ∞, respectively. It can be observed from Figure 2(f) that the convolution filter generated from the unconstrained ICA model results in much noise. (Note that the detection results of Figure 2(f) is based on the segmentation of the control limits with K = 3 in the inspection process. The use of K = 3 is to follow the typical 3-sigma standard deviation used in statistical control limits.) A control constant K = 2.5 or 3.0 generates similar and satisfactory results for the constrained ICA model. It has been found that the PSO search process cannot find a feasible solution for the constrained ICA model with a control constant K less than 2, even the number of particles and the maximum number of search iterations are respectively increased up to 50 and 5000.

In practical implementation, K = 2.5 or 3 can be used to set up the constraint. The tighter control constant K = 2.5 generally gives more noisy points but preserves a better shape and area of a detected defect in an inspection image. This is because a smaller control constant value results in tighter control limits to segment local anomalies from the uniform background in the inspection process. The tiny noisy points can be easily removed using a post-processing technique such as the morphological operations. Throughout the subsequent experiments, a control constant K = 3 is used to set up the constraint in the training process, and control limits (thresholds) in the inspection process.

3.1 Detection in low-contrast surface images

Figure 4(a1) shows a faultless backlight panel image. Figures 4(a2)-(a5) illustrate four defective surface images of backlight panels, in which the subtle defects embedded in the low-contrast surfaces are hardly visible. Figures 4(b1)-(b5) are the respective enhanced images of Figures 4(a1)-(a5) to visualize the locations and shapes

of defects. Note that the geometric structure and uneven illumination of backlight panel surfaces are also highlighted in the enhanced images. Under the control constant K = 3, the detection results from the convolution filter are demonstrated as binary images and shown in Figures 4(c1)-(c5). In the defective images of Figures 4(a2)-(a5), all hardly-visible defects are well detected. For the faultless surface image of Figure 4(a1), the resulting binary image is uniformly white and no defect is claimed. In order to demonstrate the detected shape and location of a defect in the binary image, a morphological closing is first carried out on the binary image, and then the boundary of the detected defect in the post-processing image is superimposed on the enhanced image. Figures 5(a)-(d) present the superimposed results for the four defective images in Figures 4(a2)-(a5), respectively. They show that the shape and location of each subtle defect in a low-contrast surface image can be reliably identified.

Figure 6 demonstrates further the detection results of LCD glass substrate images. Figure 6(a1) is a clear glass substrate image, and Figures 6(a2)-(a5) are four defective glass substrate images. It can be seen from the enhanced images in Figures 6(b1)-(b5) that LCD glass substrates contain a horizontal structural pattern with uneven lighting on the surfaces. Figures 6(c1)-(c5) show the detection results as binary images using the trained convolution filter and the control constant with K = 3. The detection results also reveal that all local defects embedded in low-contrast surface images can be effectively detected, and the resulting binary image of a clear surface image is approximately a uniform white image. In the following two subsections, we individually discuss the effects of changes in window size of a filter and number of training image patches on the detection results.

3.2 Effect of changes in window size

In the present study, the size of the neighborhood window is set at 20×20 pixels. The choice of a proper window size must be large enough to contain the image content in the surrounding region of each pixel. Too small a window size causes insufficient representation of common characteristics of a surface image and may generate much noise in the filtered image. However, too large a window size may over-smooth subtle defects and requires more computation time in the inspection process. In order to evaluate the effect of varying window sizes on the convoluted responses, the two defective backlight panel images shown in Figures 4(a3) and (a4) are used as the test samples. In the experiment, the window size of an image patch was varied from 10×10, 15×15, 20×20 and 25×25 pixels. All parameter values of the PSO search procedure were the same as those described previously to find the best convolution filter for each of the four window sizes.

Figures 7(a1)-(a4) and 7(b1)-(b4) show, respectively, the detection results of the two defective surface images in Figures 4(a3) and (a4) from the four window sizes. The detection results of both test images consistently reveal that the small window size 10×10 cannot reliably detect the defects and generates much random noise. The large window size 25×25 over-smoothes the small defects, and makes the detected defect pixels become scattered. Window sizes 15×15 and 20×20 generate similar detection results, and the defects in both test images are well segmented. They are recommended for the application of defect detection in low-contrast uniform surface images.

3.3 Effect of the number of training image patches

In the previous experiments, we used 100 image patches randomly selected from a faultless surface image to construct the column vectors of the data matrix in the

training process. In this subsection, we evaluate further the effect of changes in the number of training image patches. Again, the two defective backlight panel images shown in Figures 4(a3) and (a4), and the additional faultless surface image in Figure 4(a1) are used as the test samples.

The number of training image patches of size 20×20 was varied from 50, 100 to 150. All parameter values used in the PSO search procedure were the same for these three different sizes of data matrices. The detection results shown as binary images are presented in Figure 8. It is apparent from Figures 8(a1), (b1) and (c1) that the small number of 50 image patches does not provide a sufficient data matrix for training. Although the subtle defects can be still detected, they appear in a much scattering manner and much noise is generated in the filtered images. The numbers of 100 and 150 training image patches generate similar detection results, as seen in Figures 8(a2)-(a3), (b2)-(b3) and (c2)-(c3). In considering the required computation time in the training process, 100 training image patches are sufficient to construct the data matrix for the design of a convolution filter in defect detection applications.

Before the end of the Experiment section, the proposed method is also applied to the enhanced version of the low-contrast images in Figures 4 and 6, in which the defects along with the structured texture and uneven brightness are much clear. Figures 9(a1)-(a5) and (b1)-(b5) show, respectively, the detection results of the proposed method with control constant K = 2.5 for the enhanced images in Figures 4(b1)-(b5) and 6(b1)-(b5). The experimental results reveal that all defects in the test images can also be detected, but much noise is generated in the filtered images and the detected defect sizes are scattered. This is because the training images contain complicated textures in the unevenly illuminated background. The randomly selected

image patches used in training are beyond a simple translated version to each other, i.e. they may involve more than one latent source. A few independent components (i.e. a filter bank) may have to be estimated from the constrained ICA model for better detection results of the enhanced images.

A comparative experiment between the proposed method and the well-known Wiener filter [43, 44] is further given in Figures 10 and 11 based on the test samples in Figures 4(a1)-(a5) and 6(a1)-(a5). Figures 10(a1)-(a5) show the resulting images of Wiener filtering for the original images of the LCD backlight panels in Figures 4(a1)-(a5), respectively. To follow the same control limits of the proposed method, the control constant of $K = 3$ is also used for the Wiener-filtered images, and the binarized images are presented in Figures 10(b1)-(b5). Figures 11(a1)-(a5) and (b1)-(b5) present the resulting images of Wiener filtering and their binarization for the original images of the LCD glass substrates in Figures 6(a1)-(a5). The experimental results indicate that the Wiener filtering method can well detect better-contrasted anomalies, while it cannot effectively segment the subtle defects such as those shown in Figures 4(a2) and 6(a3).

4. Conclusions

Detecting small defects which appear as local anomalies embedded in a homogeneous surface is a common problem in automated surface inspection in industry. The defects under inspection are generally small in size and show no distinct intensity variations from their surrounding regions. Therefore, simple thresholding and gradient-based methods cannot be reliably applied to identify such defects in low-contrast surface images. In this study, we have presented a filtering approach for

defect detection in low-contrast surface images. The characteristic of each pixel in the inspection image is measured by the impulse response which is obtained by the convolution of the image with a specifically designed filter.

A constrained ICA model has been proposed for the design of the convolution filter. The objective of the ICA model is based on the maximization of negentropy with the constraint that all resulting source values from the training image patches are within statistical control limits. The ICA objective makes the convolution filter have the most representative source intensity of a training surface image, while the constraint in the ICA model confines the variation of source values from all training image patches within a satisfactory level. The merit of the constraint in the ICA model is that the same control constant K selected in the training process is also used to set up the control limits for segmenting local anomalies from the uniform background in the inspection process. This eliminates the tiresome and unreliable try-and-error approach to determine the threshold values for segmentation.

Since the images of the object surfaces studied in this paper can be considered as having a uniform intensity, all image patches anywhere in a defect-free surface are considered to be identical. The training image patches entered as column vectors in the data matrix are then the translated versions of the same source signal. Therefore, it is enough to estimate just one source component and its corresponding de-mixing row vector. The resulting de-mixing vector that satisfies the constraint in the ICA model is used as the convolution filter. PSO that uses a group of particles to simultaneously and dynamically search for local best positions and the global position is applied to solve for the constrained ICA model. Experimental results showed that the PSO search procedure can effectively find a feasible solution involving hundreds of continuous

decision variables in a moderate number of iterations.

The convolution filter derived from the constrained ICA model will give an impulse response within the control limits when the filter spans a faultless region in the inspection image, and will generate a distinct impulse response outside the control limits for a defective region. Experimental results from the backlight panels and LCD glass substrates have shown that the proposed ICA-based filtering scheme can effectively detect various small defects in low-contrast surface images. It is concluded from the experiments that the following parameter setup can generate good detection results for defect inspection in uniform surface images. For the PSO search algorithm, population size t = 10, positive weights $c_1 = c_2 = 2$, and number of iterations = 200. For the constrained ICA model, number of training image patches = 100, image patch size = 20×20, and control constant K = 2.5 or 3.

Although the proposed method currently aims at defect detection in uniform surface images, it is believed that it can be easily extended to the inspection of defects in homogeneous texture images. A homogeneous texture will show self-similarity property in the image, which means all sufficiently large image patches are similar to each other, regardless of their positions in the textured image. If all training image patches in a faultless textured image can be considered as the translated versions of the original texture pattern, the proposed constrained ICA model can then be used to design a single convolution filter for distinguishing local anomalies from the homogeneous texture background.

References

1. J. Wilder, Finding and evaluating defects in glass, In: Machine Vision for Inspection and Measurement, H. Freeman (Ed.), Academic Press, New York, NY, 1989, p. 237.

2. J. Olsson, S. Gruber, Web process inspection using neural classification of scattering light, Proceedings of the IEEE International Conference on Industrial Electronics, Control, Instrumentation and Automation (IECON'92), 1992, pp. 1443-1448.

3. C. Fernandez, D. Platero, P. Campoy, R. Aracil, Vision system for on-line surface inspection in aluminum casting process, Proceedings of the IEEE International Conference on Industrial Electronics, Control, Instrumentation and Automation (IECON'93), 1993, pp. 1854-1859.

4. D. Brzakovic, N. Vujovic, Designing defect classification system: a case study, Pattern Recognition 29 (1996) 1401-1419.

5. K. V. Ramana, B. Ramamoorthy, Statistical methods to compare the texture features of machine surfaces, Pattern Recognition 29 (1996) 1447-1459.

6. W.-S. Kim, D.-M. Kwak, Y.-C Song, D.-H. Choi, K.-H. Park, Detection of spot-type defects on liquid crystal display modules, Key Engineering Materials 270-273 (2004) 808-813.

7. F. Saitoh, Boundary extraction of brightness unevenness on LCD display using genetic algorithm based on perceptive grouping factors, Proceedings of the International Conference on Image Processing, Kobe, Japan, 1999, pp. 308-312.

8. B. C. Jiang, C.-C. Wang, H.-C. Liu, Liquid crystal display surface uniformity defect inspection using analysis of variance and exponentially weighted moving average techniques, International Journal of Production Research 43 (2005) 67-80.

9. S. M. Sokolov, A. S. Treskunov, Automatic vision system for final test of liquid crystal display, Proceedings of the IEEE International Conference on Robotics and Automation, Nice, France, 1992, pp. 1578-1582.

10. J. Y. Lee, S. I. Yoo, Automatic detection of region-mura defect in TFT-LCD, IEICE Trans. Inf. and Syst. E87-D (2004) 2371-2378.

11. T. W. Lee, Independent Component Analysis: Theory and Application, Kluwer

Academic Publishers, Boston, MA, 1998.

12. A. Hyvarinen, J. Karhunen, E. Oja, Independent Component Analysis, John Wiley and Sons, New York, NY, 2001.

13. S. Ikeda, K. Toyama, Independent component analysis for noisy data-MEG data analysis, Neural Networks 13 (2000) 1063-1074.

14. R. Vigario, J. Sarela, V. Jousmaki, M. Hamalainen, E. Oja, Independent component approach to the analysis of EEG and MEG recordings, IEEE Trans. Biomedical Engineering 47 (2000) 589-593.

15. T. P. Jung, S. Makeig, M. J. McKeown, A. J. Bell, T. W. Lee, T. J. Sejnowski, Imaging brain dynamics using independent component analysis, Proceedings of the IEEE 89 (2001) 1107-1122.

16. C. J. James, O. J. Gibson, Temporally constrained ICA: an application to artifact rejection in electromagnetic brain signal analysis, IEEE Trans. Biomedical Engineering 50 (2003) 1108-1116.

17. C. F. Beckmann, S. M. Smith, Probabilistic independent component analysis for functional magnetic resonance imaging, IEEE Trans. Medical Imaging 23 (2004) 137-152.

18. Y. Deville, L. Andry, Application of blind source separation techniques to multi-tag contactless identification systems, IEICE Trans. Fundamentals of Electronics, Communications and Computer Sciences E79-A (1996) 1694-1699.

19. H. M. Park, H. Y. Jung, T. W. Lee, S. Y. Lee, On subband-based blind signal separation for noisy speech recognition, Electronic Letters 35 (1999) 2011-2012.

20. M. S. Bartlett, J. R. Movellan, T. J. Sejnowski, Face recognition by independent component analysis, IEEE Trans. Neural Networks 13 (2002) 1450-1464.

21. P. C. Yuen, J. H. Lai, Face representation using independent component analysis, Pattern Recognition 35 (2002) 1247-1257.

22. O. Deniz, M. Castrillon, M. Hernandez, Face recognition using independent component analysis and support vector machines, Pattern Recognition Letters 24 (2003) 2153-2157.

23. T. K. Kim, H. Kim, W. Hwang, J. Kittler, Independent component analysis in a local facial residue space for face recognition, Pattern Recognition 37 (2004) 1873-1885.

24. R. Manduchi, J. Portilla, Independent component analysis of textures, Proceedings of the IEEE International Conference on Computer Vision, Kerkyra, Greece, 1999, pp. 1054-1060..

25. Y. W. Chen, X. Y. Zeng, H. Lu, Edge detection and texture segmentation based on independent component analysis, Proceedings of the 16th International Conference on Pattern Recognition, Quebec City, Canada, 2002, pp. 351-354.

26. R. Jenssen, T. Eltoft, Independent component analysis for texture segmentation, Pattern Recognition 36 (2003) 2301-2315.

27. A. Hyvarinen, P. Hoyer, E. Oja, Sparse code shrinkage for image denoising, Proceedings of the IEEE International Joint Conference on Neural Networks, Ahchorage, Alaska, 1998, pp. 859-864.

28. A. Hyvarinen, P. Hoyer, E. Oja, Image denoising by sparse code shrinkage, In: Intelligent Signal Processing, S. Haykin, B. Kosko (Eds.), IEEE Press, New York, NY, 2001, pp. 554-568.

29. A. Hyvarinen, Sparse code shrinkage: denoising of nongaussian data by maximum likelihood estimation, Neural Computation 11 (1999) 1739-1768.

30. Y. Hung, S. Luo, A dynamic denoising natural image compression, Proceedings of the International Conference on Signal Processing, Beijing, China, 2002, pp. 1179-1182.

31. A. Hyvarinen, E. Oja, Independent component analysis: algorithms and applications, Neural Networks 13 (2000) 411-430.

32. A. J. Bell, T. J. Sejnowski, An information-maximization approach to blind separation and blind deconvolution, Neural Computation 7 (1995) 1129-1159.

33. A. Amari, A. Cichocki, H. Yang, A new learning algorithm for blind source separation, In: Advances in Neural Information Processing Systems, D. Touretzky, M. Mozer, M. Hasselmo (Eds.), MIT Press, Cambridge, MA, 1996, pp. 757-763.

34. A. Hyvarinen, E. Oja, A fast fixed-point algorithm for independent component analysis, Neural Computation 9 (1997) 1483-1492.

35. A. Hyvarinen, Fast and robust fixed-point algorithms for independent component analysis, IEEE Trans. Neural Networks 10 (1999) 626-634.

36. J. Kennedy, R. Eberhart, Particle swarm optimization, Proceedings of the IEEE International Conference on Neural Networks, Perth, Australia, 1995, pp.

1942-1948.

37. H. Yoshida, K. Kawata, Y. Fukuyama, S. Takayama, Y. Nakanishi, A particle swarm optimization for reactive power and voltage control considering voltage security assessment, IEEE Power Syst. 15 (2000) 1232-1239.

38. M. Clerc, J. Kennedy, The particle swarm-explosion, stability and convergence in a multidimensional complex space, IEEE Trans. Evol. Comput. 6 (2002) 58-73.

39. R. Mendes, P. Cortez, M. Rocha, J. Neves, Particle swarms for feedforward neural network training, Proceedings of the International Joint Conference on Neural Networks, Honolulu, Hawaii, 2002, pp. 1895-1899.

40. Z.-L. Gaing, Particle swarm optimization to solving the economic dispatch considering the generator constraints, IEEE Trans. Power Syst. 18 (2003) 1187-115.

41. Y. Shi, R. Eberhart, A modified particle swarm optimizer, Proceedings of the IEEE International Conference on Evolutionary Computation, Anchorage, Alaska, 1998, pp. 69-73.

42. J. Kennedy, The particle swarm: social adaptation of knowledge, Proceedings of the IEEE International Conference on Evolutionary Computation, Piscataway, NJ, 1997, pp. 303-308.

43. D. T. Kuan, A. A. Sawchuk, T. C. Strand, P. Chavel, Adaptive noise smoothing filter for images with signal-dependent noise, IEEE Trans. Pattern Anal. Mach. Intel. 7 (1985) 165-177.

44. M. Das, P. Ramuhalli, L. Udpa, S. Udpa, An adaptive Wiener filter based technique for automated detection of defect locations from bobbin coil eddy current data, AIP (American Institute of Physics) Conference Proceedings, Vol. 615, 2002, pp. 639-646.

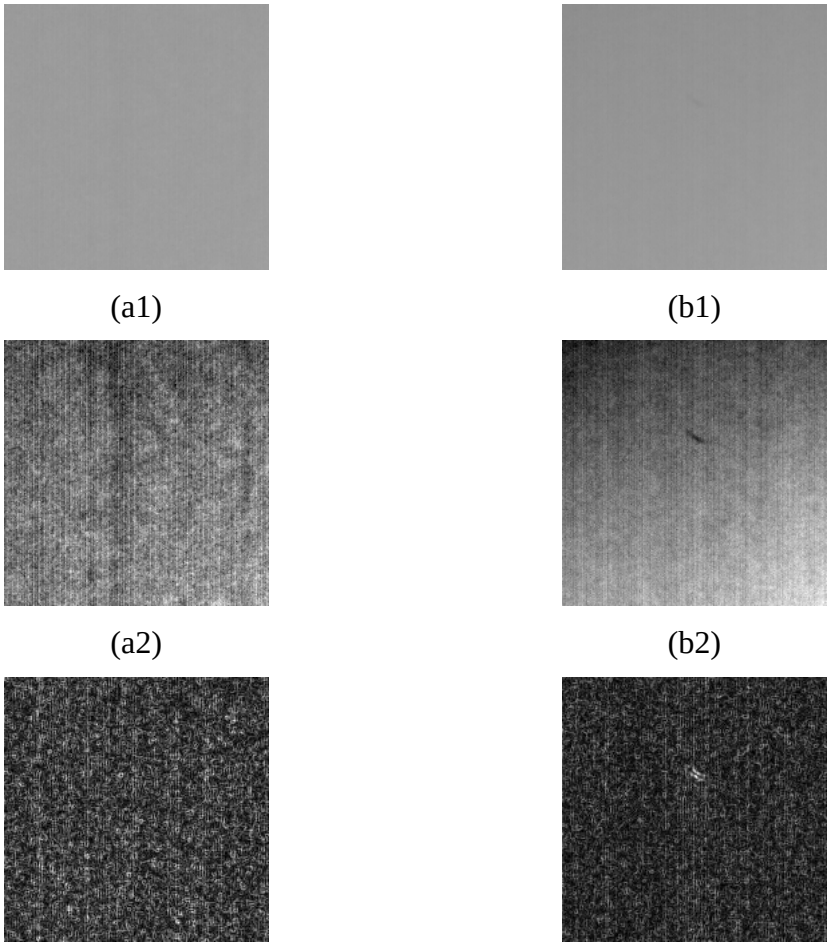

Figure 1. Low-contrast sample images of LCD backlight panels: (a1) faultless surface image; (b1) defective surface image; (a2), (b2) respective enhanced images; (a3), (b3) respective gradient images.

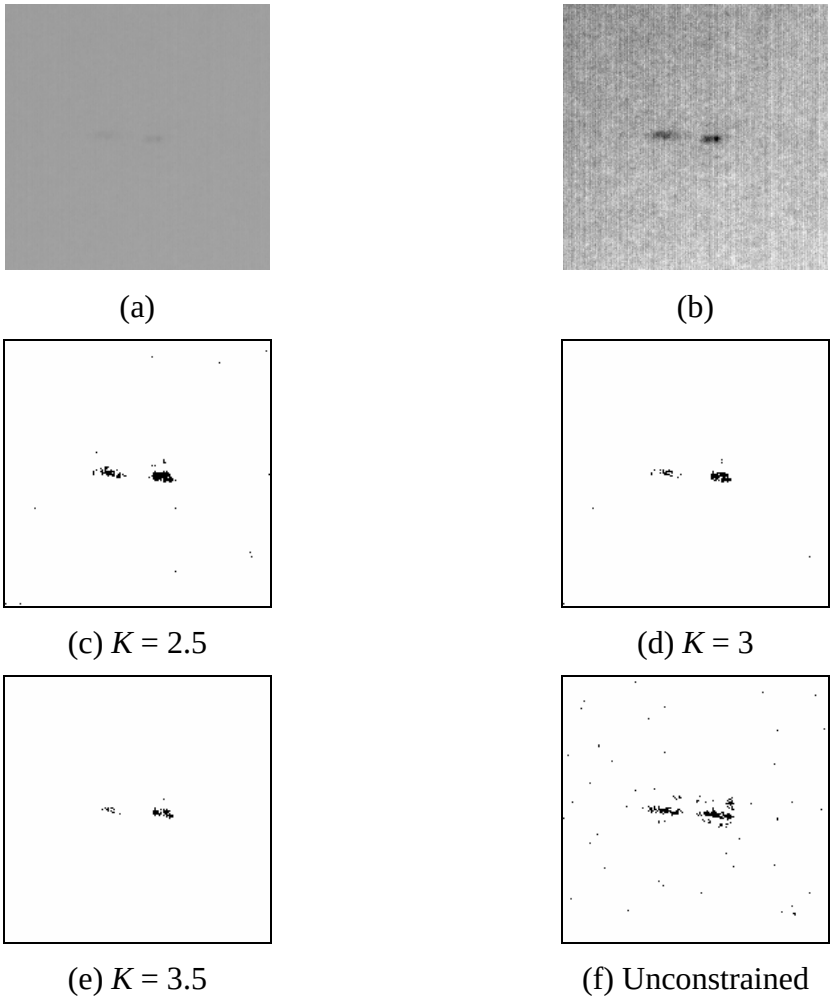

Figure 2. Effect of varying control constant K in training: (a) original image of a defective backlight panel; (b) enhanced image of (a) to show the defect in the surface; (c)-(f) detection results as binary images from the control constant K = 2.5, 3, 3.5 and infinite, respectively.

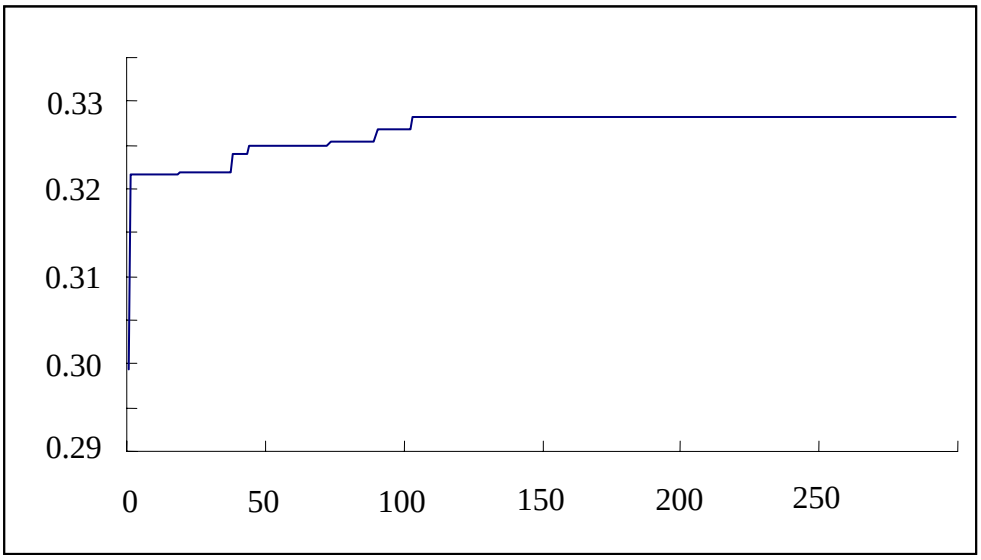

Figure 3. Plot of the fitness value with respect to the number of iterations, which shows the convergence of the PSO search procedure for the backlight panel image in the constrained ICA model.

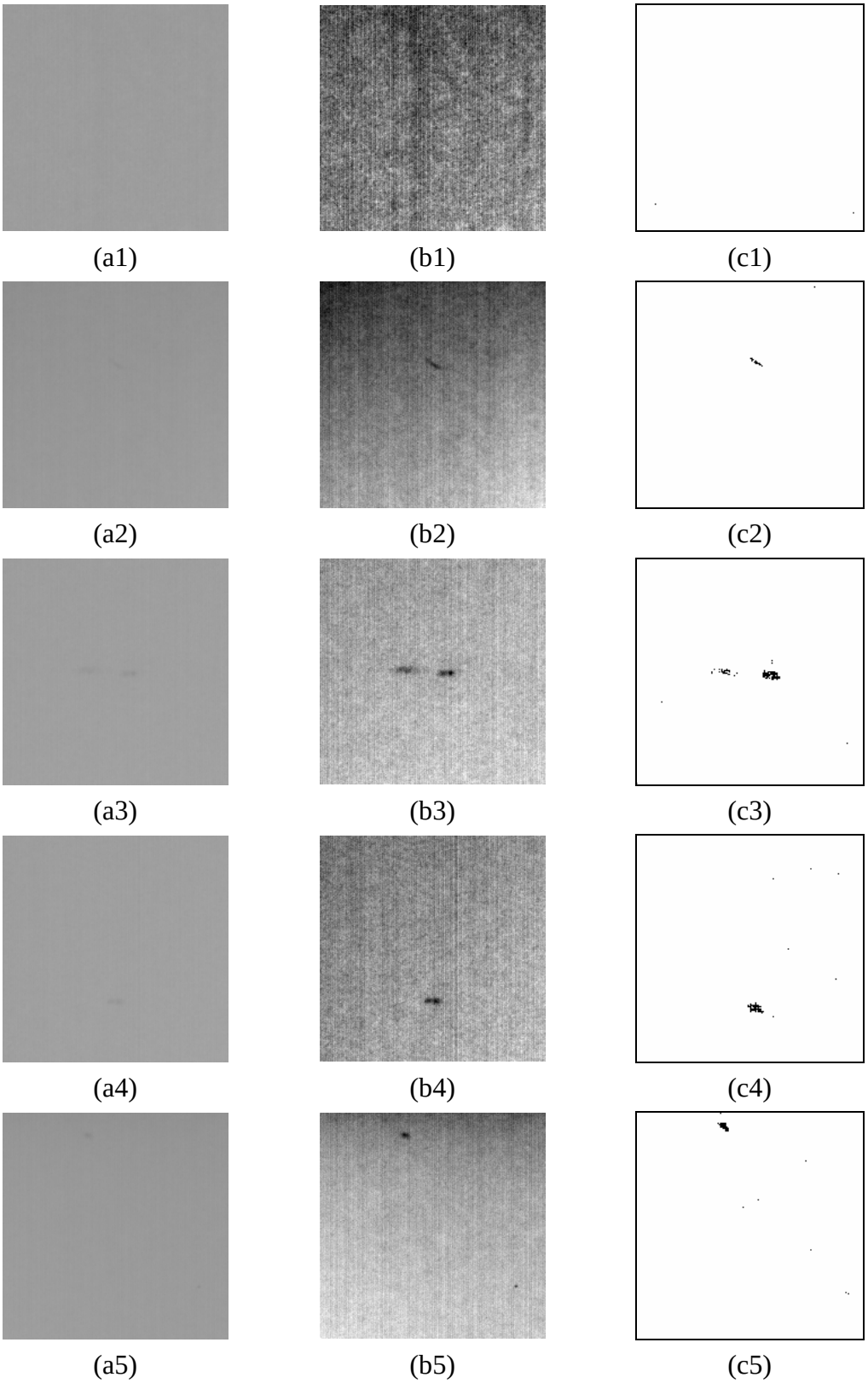

Figure 4. Detection results of LCD backlight panels: (a1)-(a5) a clear and four defective surface images; (b1)-(b5) respective enhanced images of (a1)-(a5); (c1)-(c5) respective resulting binary images for defect segmentation.

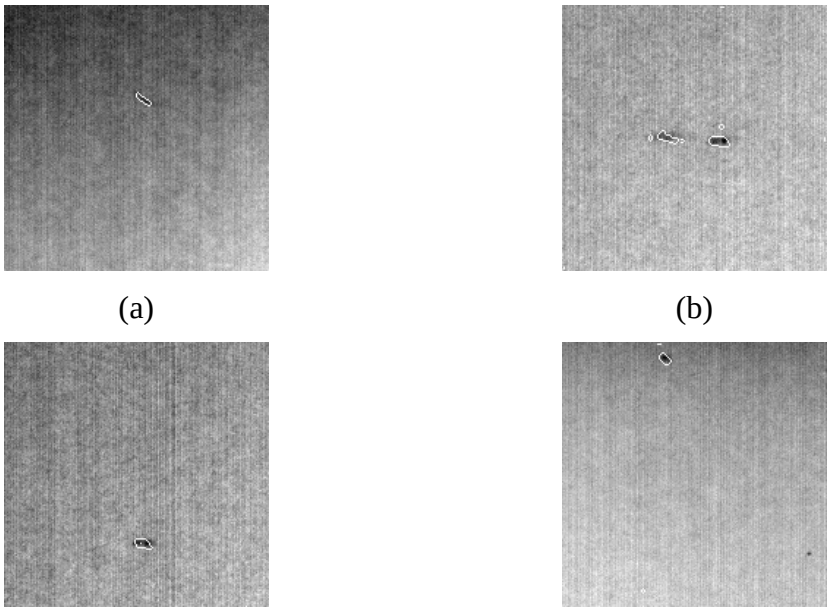

(a) (b)

(c) (d)

Figure 5. (a)-(d) Superimposing boundaries of detected defect areas on the enhanced images for the defective backlight panel surfaces in Figures 4(a2)-(a5), respectively.

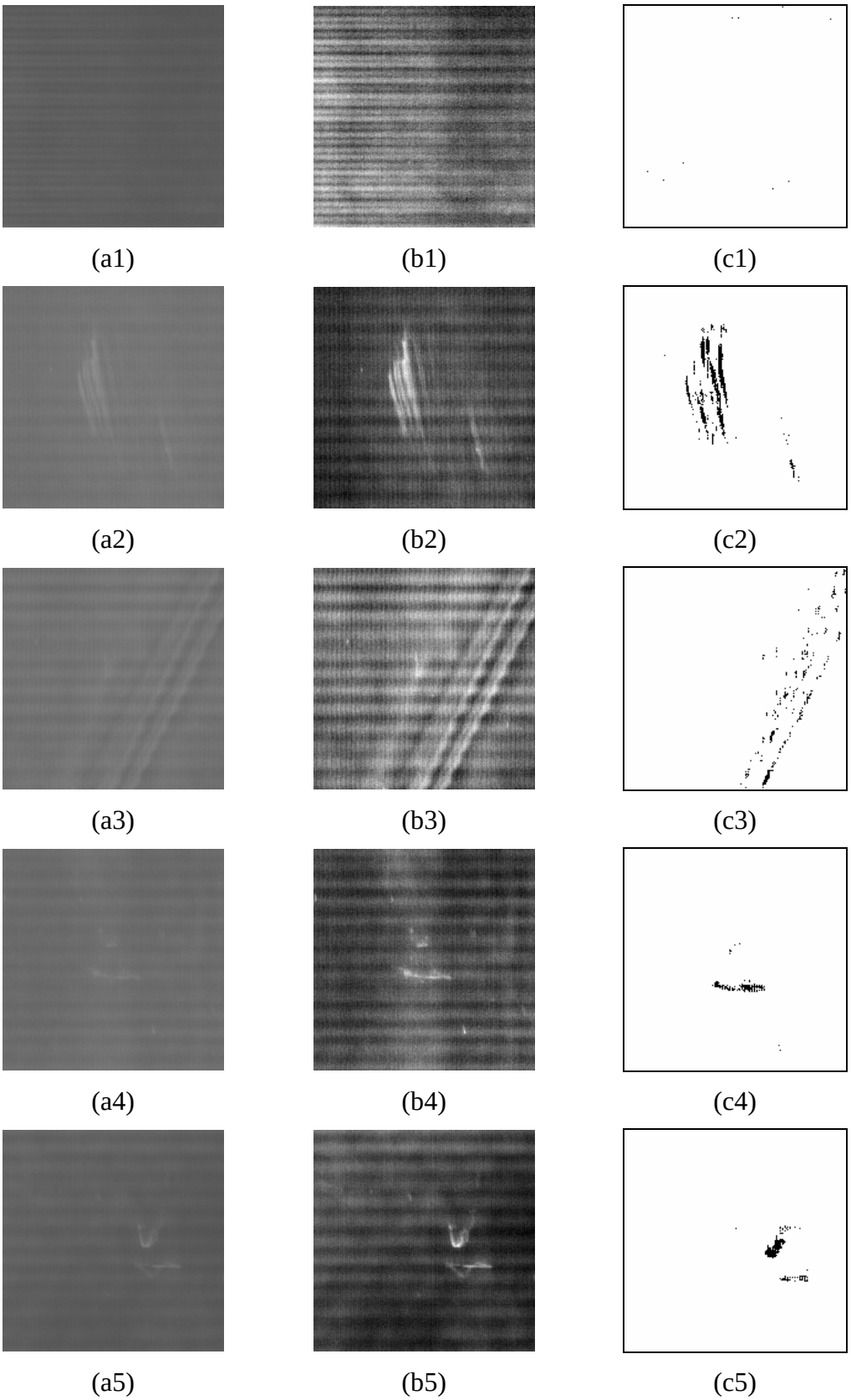

Figure 6. Detection results of LCD glass substrates: (a1)-(a5) a clear and four defective surface images; (b1)-(b5) respective enhanced images; (c1)-(c5) respective resulting binary images for defect segmentation.

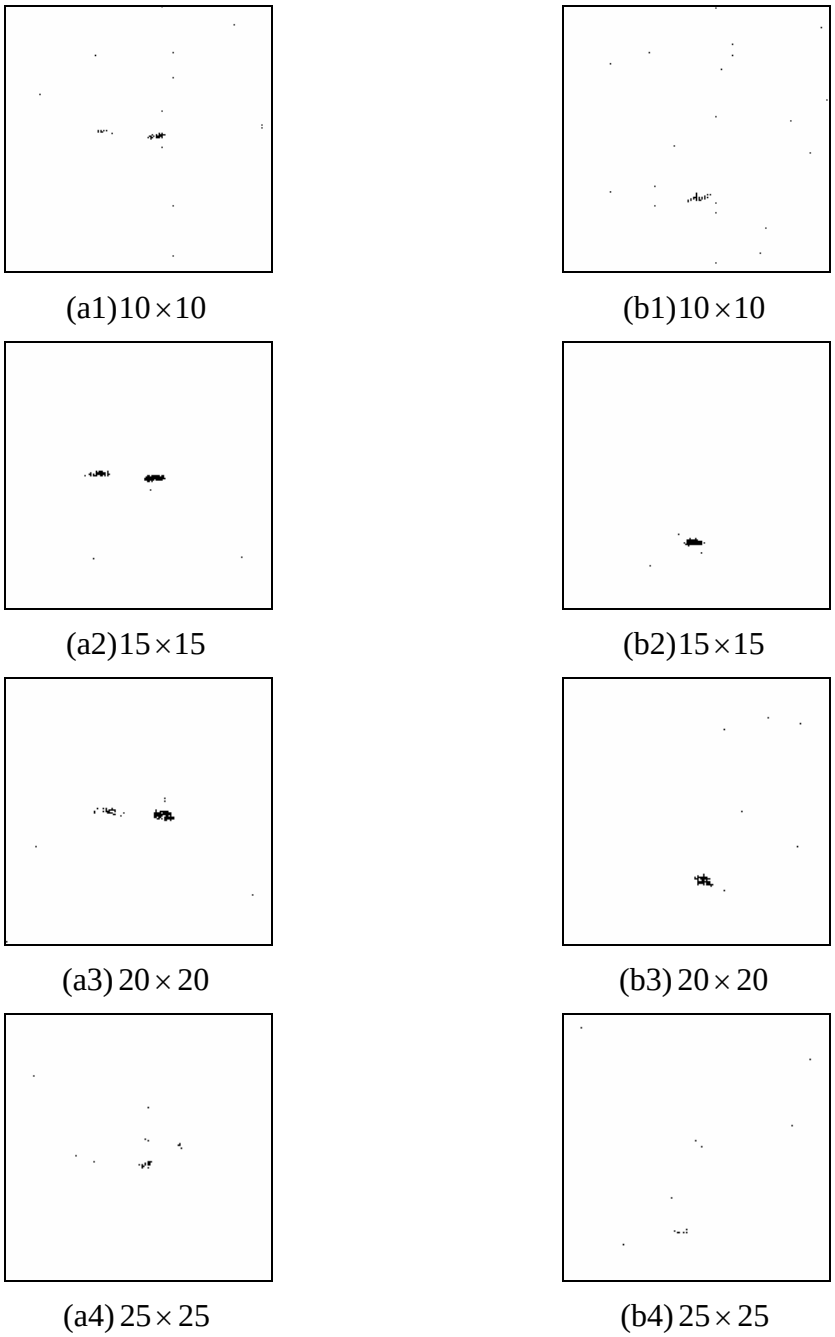

Figure 7. Effect of changes in window size: (a1)-(a4) detection results from window sizes 10×10, 15×15, 20×20 and 25×25 for the defective backlight panel image in Figure 4(a3); (b1)-(b4) detection results from the respective window sizes for the defective panel image in Figure 4(a4).

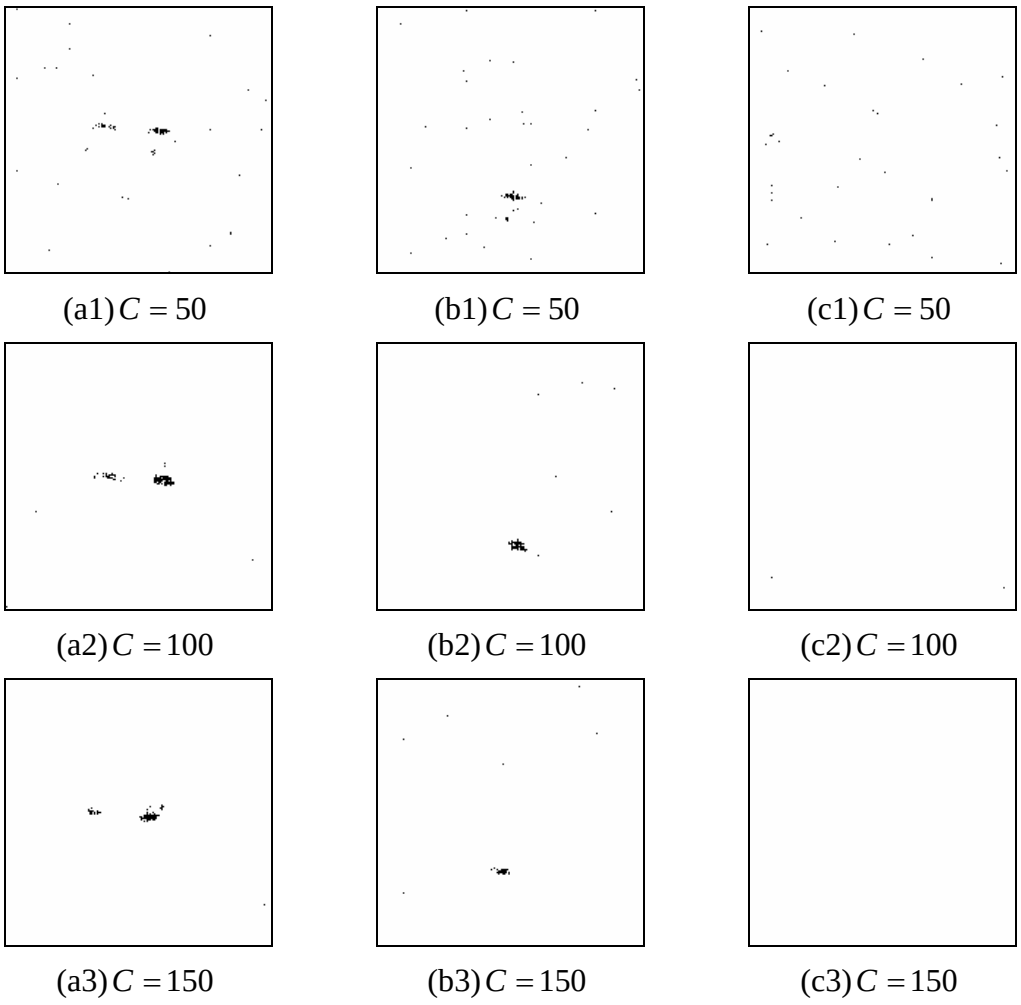

Figure 8. Effect of changes in the number of training image patches *C*: (a1)-(a3) detection results from $C = 50$, 100 and 150 for the defective backlight panel image in Figure 4(a3); (b1)-(b3) detection results from $C = 50$, 100 and 150 for the defective image in Figure 4(a4); (c1)-(c3) detection results from $C = 50$, 100 and 150 for the faultless image in Figure 4(a1).

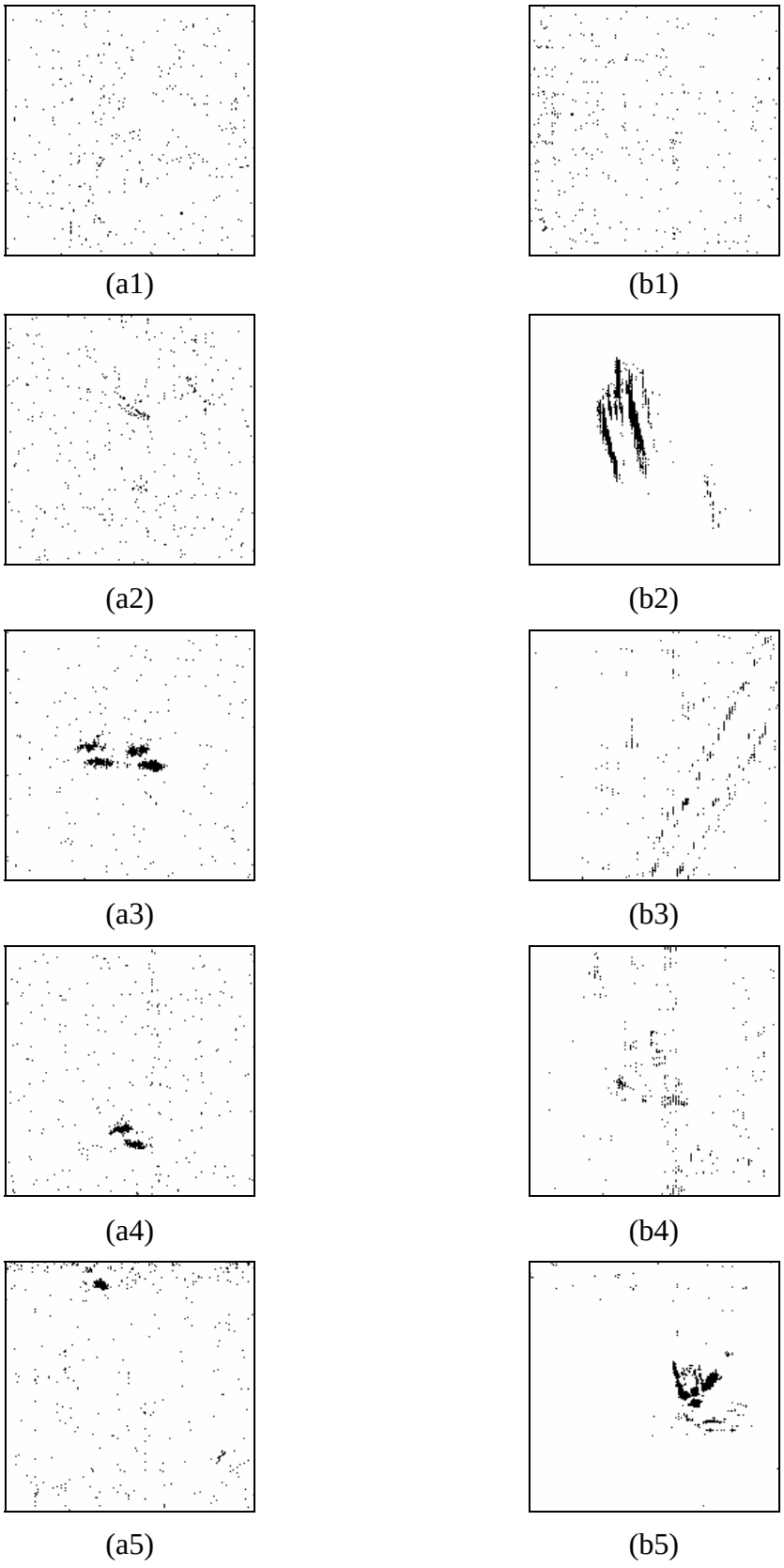

Figure 9. (a1)-(a5) Respective detection results of the enhanced images in Figure 4(b1)-(b5); (b1)-(b5) respective detection results of the enhanced images in Figure 6(b1)-(b5). (The control constant is at $K = 2.5$.)

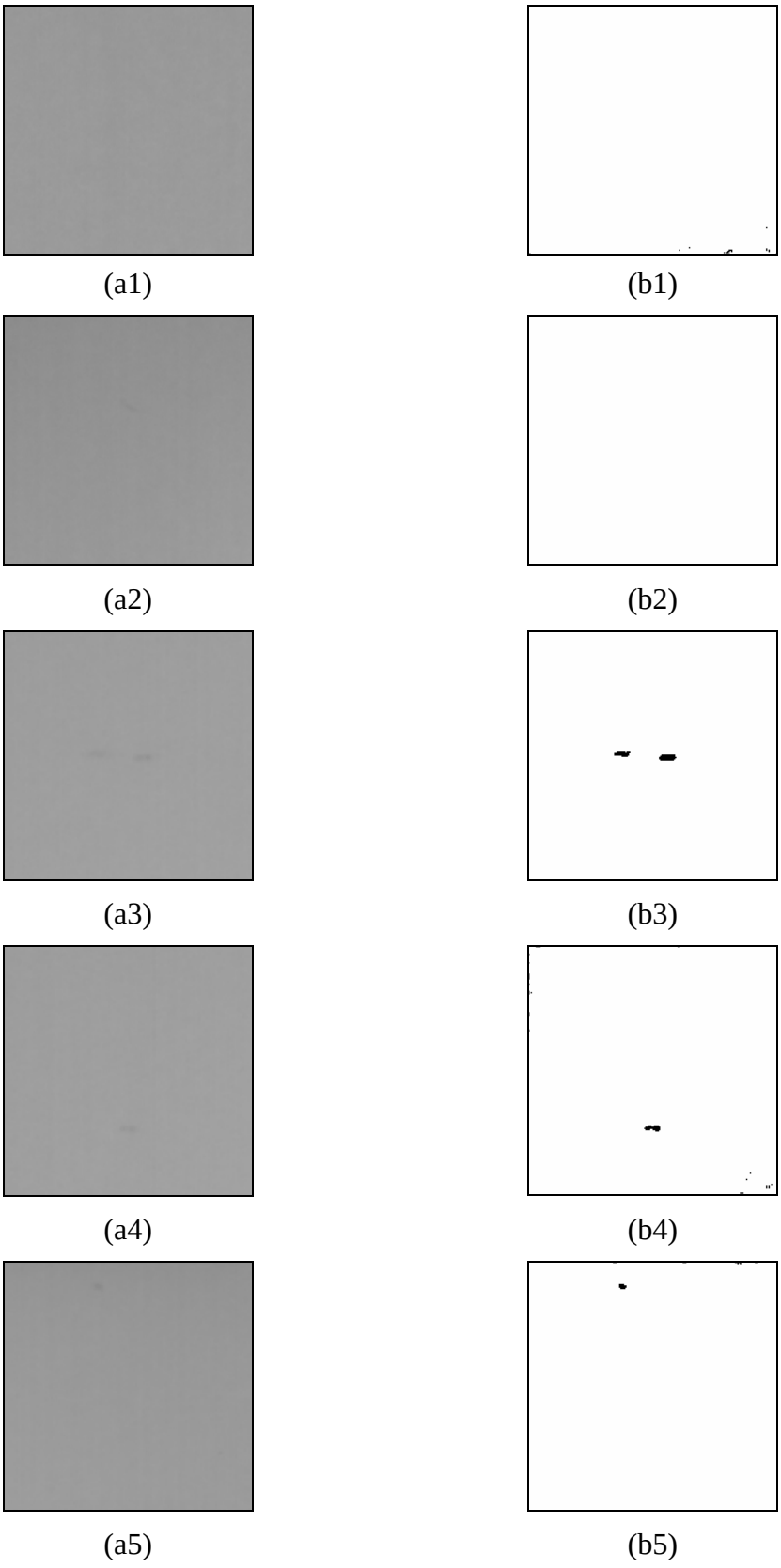

Figure 10. (a1)-(a5) Respective Wiener-filtered images of the LCD backlight panels in Figures 4(a1)-(a5); (b1)-(b5) respective binarized images of (a1)-(a5) from the 3-sigma control limits.

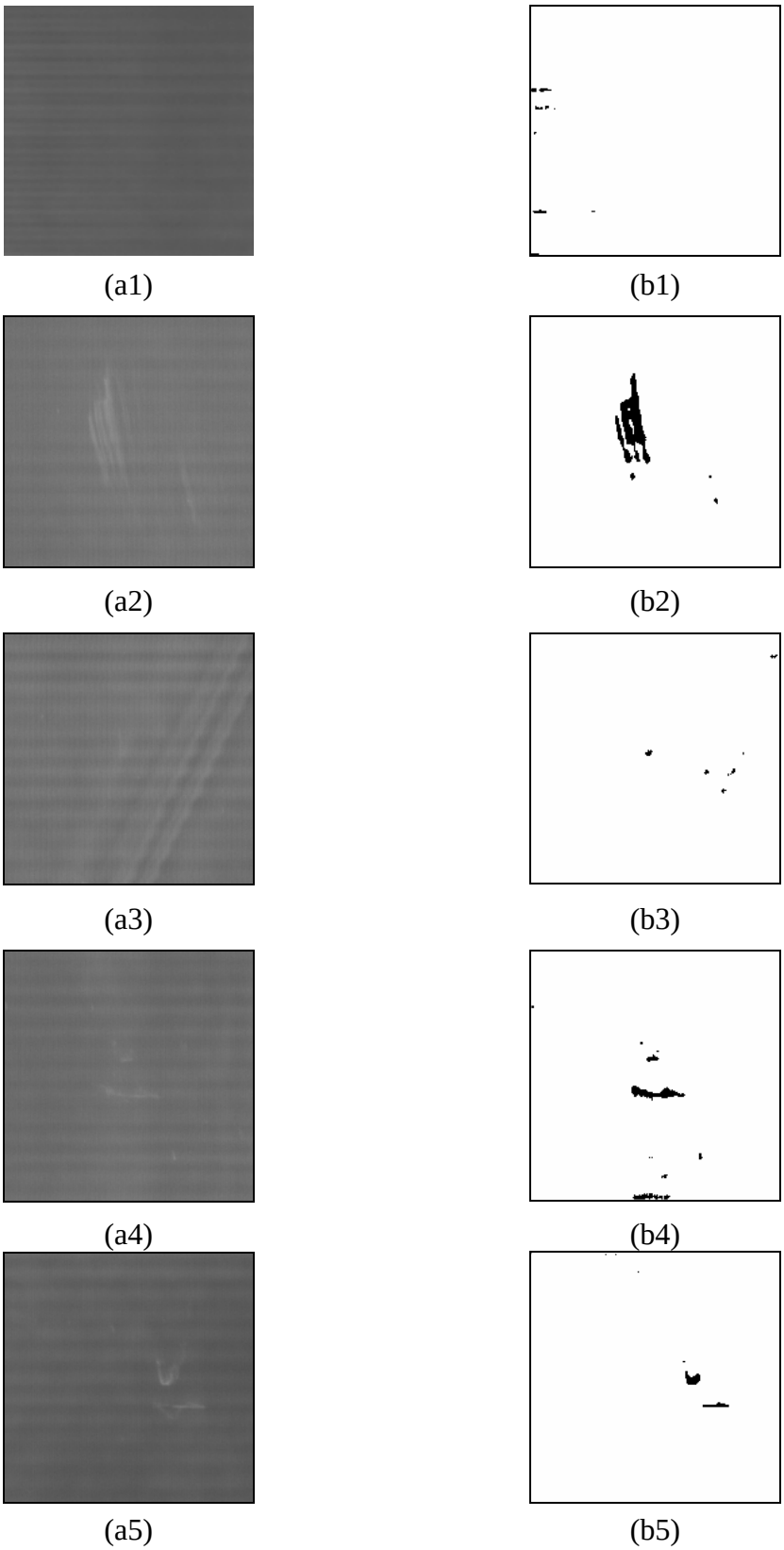

Figure 11. (a1)-(a5) Respective Wiener-filtered images of the LCD glass substrates in Figures 6(a1)-(a5); (b1)-(b5) respective binarized images of (a1)-(a5) from the 3-sigma control limits.